On the Use of Metallized Cavities in Printed Slot Arrays with Dielectric Substrates

ROBERT J. MAILLOUX, FELLOW, IEEE

Abstract—**A detailed analysis of infinite slot arrays excited by delta-function current sources is presented. The existence of severe array blindness is proved for most of the cases of slots without metallic cavity separators.**

I. Introduction

MOST FLAT PLATE slot arrays produce a pencil beam radiation pattern with a stationary (nonscanning) beam direction. In order to maintain proper impedance match over useful frequency ranges, it is common practice in the design of nonscanning arrays to isolate the slot elements from internal coupling through the parallel plate feed structure by the use of metallic walls between elements. Such a configuration, as shown in Fig. 1(b), might have walls formed by milling the cavities from a metal block, or by the use of pins or plating through holes in the ground planes and supporting dielectric material.

The recent success of printed microstrip arrays has kindled an interest in consideration of the structure shown in Fig. 1(a), where there are no cavity walls to provide internal isolation between adjacent slots. This interest has grown because of the need to investigate new scanning array architectures for layered monolithic fabrication using high dielectric or semiconductor substrates.

The purpose of this paper is to compare the radiation properties of the array geometries of Fig. 1(a) (case A) and Fig. 1(b) (case B) for an infinite array in order to determine whether it is realistic to consider scanning arrays without metallized cavity construction.

It should be noted that the authors of a recent paper [1] on the scanning properties of dipole arrays with dielectric layers and a ground screen attempted to include slot arrays similar to that of case A by an application of duality. Such application is incorrect even for the slot array with dielectric layers, but when a second ground screen is added (with or without dielectric layers), the slotted screen introduces a new boundary condition that cannot be addressed by generalization of duality. In the present analysis the Green's functions for both regions are chosen to satisfy the boundary conditions at the slotted screen and the ground screen, and only a single integral equation is needed at each slot.

Manuscript received September 6, 1985; revised March 10, 1986.
The author is with the Electromagnetic Sciences Division, RADC/EEAA, Hanscom Air Force Base, MA 01731.
IEEE Log Number 8613890.

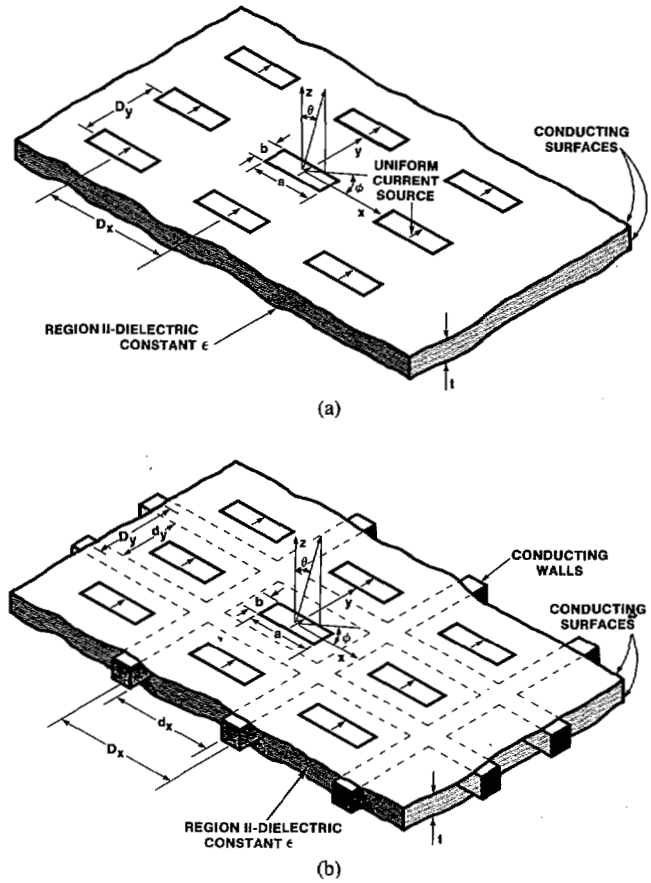

Fig. 1. Array geometries. (a) Case A: slot array without internal cavities. (b) Case B: slot array with internal cavities.

II. The Mathematical and Physical Models

In order to perform a comparison that isolates effects due to modes within the dielectric loaded region, it was necessary to use the same source function for the slots in both cases. This led to the assumption of a delta-function current source at the center of each slot. The current source is assumed constant across each slot, and associated entirely with a discontinuity in the tangential x directed magnetic field, so that the line integral for this scattered field is

$$I = -\int H \cdot dl \tag{1}$$

around the vanishing cross section of the current source reduces to

$$B_x^1 - B_x^2 = -\mu I_0 \delta(x), \qquad -b/2 \leqslant y \leqslant b/2 \tag{2}$$

U.S. Government work not protected by U.S. copyright

at the slot with center $(x, y) = (0, 0)$, with $\delta(x)$ the dirac delta function.

Consistent with the assumption of constant impressed current as a function of the coordinate "y," is the restriction of narrow slot dimensions "b," and later the neglect of all field variations in "y" across the slots. This model is taken as a realistic approximation to the excitation by a thin wire carrying constant current, a common method of exciting slots in a flat-plate configuration. The model is the Babinet equivalent of the delta-function voltage excitation model for dipoles, and should have similar convergence properties [2]. The model is the same as used by Galejs [3] for a single slot problem.

All other slots are excited by a similar current source, related to the above by a progressive phase relationship, so that the slot with center location $(x_m, y_n) = (mD_x, nD_y)$ has current

$$I(x+mD_x, y+nD_y) = I_0 e^{-jk_0(u_0 mD_x + v_0 nD_y)} \cdot \delta(x-mD_x)\, w(y-nD_y) \quad (3)$$

where

$$w(y-nD_y) = 1 \qquad (-b/2) \le y \le b/2$$
$$0 \quad |y| > b/2.$$

In this case u_0 and v_0 are the direction cosines of the scan angle (θ_0, ϕ_0)

$$u_o = \sin\theta_0 \cos\phi_0 \quad v_0 = \sin\theta_0 \sin\phi_0. \quad (4)$$

The fields in the free space half-space (region 1) and the dielectric loaded volume below the ground plane ($z < 0$; region 2) are written in terms of scalar magnetic potential functions derived from the y directed aperture fields in the slots using Green's functions that will be given later. Fields in specific regions 1 and 2 will be later denoted by superscripts.

$$\bar{B}(r) = \nabla(\nabla \cdot \bar{\pi}_m) + k_\epsilon^2 \bar{\pi}_m$$
$$\bar{E}(r) = -j\omega\nabla \times \bar{\pi}_m. \quad (5)$$

Here the magnetic potential $\bar{\pi}_m = \hat{x}\pi$ is assumed to be a single component of a vector for the case of very thin slots (and so $E_x \cong 0$).

The Green's functions chosen to derive these scalar magnetic potential functions have zero normal derivatives at the ground screen, and so $E_y|_{z=0} \equiv 0$ except in the apertures. In addition, they must have the same periodicity as the current distribution (4) except for the case of fields within a walled cavity region, where the boundary conditions are not periodic.

In either case, the Green's functions due to a single source at (x', y', z') satisfy the inhomogeneous Helmholtz equation.

$$(\nabla^2 + k_\epsilon^2) G(r, r') = -\delta(x-x')\delta(y-y')\delta(z-z') \quad (6)$$

where

$$k_\epsilon^2 = \omega^2 \mu_0 \epsilon_\epsilon$$

Using Green's theorem to relate the functions π and G in any closed region of space to their normal derivatives at the enclosing surface, one obtains

$$\int_{v'} (\pi(r')\nabla^2 G(r, r') - G(r, r')\nabla^2\pi(r'))\, dv'$$
$$= \int_{s'} \left(\pi(r') \frac{\partial G(r, r')}{\partial \eta'} - G(r, r') \frac{\partial \pi(r')}{\partial \eta'} \right) ds' \quad (7)$$

where η' is the outward normal to the surface.

Adding and subtracting $[k_\epsilon^2 G(r, r')\pi(r')]$ within the volume integral, and using the inhomogeneous Helmholtz equation (6), one obtains an expression valid in both regions

$$\pi(r) = \int_{s'} G(r, r') \frac{\partial \pi(r')}{\partial \eta'} ds' \quad (8)$$

for the specific case in which G is chosen to have a vanishing normal derivative at the surfaces. This expression reduces to the following relationship involving tangential E-fields:

$$\text{region 1} \quad \pi^{(1)}_{(r)} = -\frac{j}{\omega} \int G'(r, r') E_y(r')\, ds' \quad (9)$$

$$\text{region 2} \quad \pi^{(2)}_{(r)} = +\frac{j}{\omega} \int G^2(r, r') E_y(r')\, ds'. \quad (10)$$

These expressions for $\pi^{(1)}$ and $\pi^{(2)}$ fully define the fields in regions 1 and 2 based upon integrals of the unknown tangential aperture fields E_y. The Green's functions $G^{(1)}$ and $G^{(2)}$ are constructed to satisfy the inhomogenous Helmholtz equation (6) and the boundary conditions on both sides of the ground screen ($z = 0$).

Since the fields on either side of the apertures are constructed from the tangential electric field, only the equation of the tangential magnetic field B_x ((2) is necessary to satisfy all continuity conditions. Equation (2) becomes (at the element with center (0, 0))

$$(\partial_{xx}^2 + k_0^2)\pi^{(1)} - (\partial_{xx}^2 + k_\epsilon^2)\pi^{(2)} = -\mu_0 I_0 \delta(x-mD_x) e^{-jk_0(u_0 mD_x + v_0 nD_y)} \quad (11)$$

with

$$-b/2 \le y \le b/2$$

for (x, y) in any aperture.

Since the total field will have the same periodicity as the assumed current excitation, one can account for this progressive phase term explicitly, and it is only necessary to satisfy the above equation or the defining equation for the Green's function (6) within the periodic cell with center $(x, y) = (0, 0)$.

III. Solution of the Integrodifferential Equation

Equation (11) is recast into the form below, where it is evidently a linear, inhomogeneous integrodifferential equation

$$(\partial_{xx}^2 + k_0^2)(\pi^{(1)} - \pi^{(2)}) = -\mu_0 I_0 \delta(x-mD_x) + k_0^2(\epsilon_r - 1)\pi^{(2)} \quad \frac{-b}{2} \le y \le \frac{b}{2} \quad (12)$$

which, for the aperture at the origin of the coordinate system can be solved in two regions $x \geqslant 0$ and $x \leqslant 0$.

$$\begin{aligned}\pi^{(1)}-\pi^{(2)} &= C_1 \cos k_0 x + C_2 \sin k_0 x \\ &\quad + \frac{1}{k_0}\int_{x_1}^{x} [-\mu_0 I_0 \delta(\zeta) + k_0^2(\epsilon_r - 1)\pi^{(2)}(\zeta)] \\ &\quad \cdot \sin k_0(x-\zeta)\, d\zeta, \qquad x \leq 0 \\ &= C_3 \cos k_0 x \\ &\quad + C_4 \sin k_0 x + \frac{1}{k_0}\int_{x_1}^{x} [+\mu_0 I_0 \delta(\zeta) \\ &\quad + k_0^2(\epsilon_r - 1)\pi^{(2)}(\zeta)] \\ &\quad \cdot \sin k_0(x-\zeta)\, d\zeta, \qquad x \leq 0. \end{aligned} \tag{13}$$

This set of integral equations applies for either case A or case B; only the choice of Green's function is different in the two regions.

A more convenient form is obtained by redefining the constant C_2, and evaluating C_4 in terms of C_2 after performing the delta function integral. This is done by integrating (13) over the source (defined to exist for some small region $\sigma \geqslant x \geqslant 0$), and then identifying the discontinuity in the first derivative of this potential difference as the source strength $-\mu I_0$, or

$$\begin{aligned}\partial_x(\pi^1(x)-\pi^2(x))|_{x=\sigma} - \partial_x(\pi^1(x)-\pi^2(x))|_{x=0} \\ = k_0(C_2 - C_4) - \mu_0 I_0 = -\mu_0 I_0\end{aligned}$$

which leads to the condition $C_2 = C_4$.

The resulting equation can be written for all "x" as

$$\begin{aligned}\pi^{(1)}-\pi^{(2)} &= C_1(1+\operatorname{sgn}(x)) \cos k_0 x + C_2 \sin k_0 x \\ &\quad + C_3(1-\operatorname{sgn}(x)) \cos k_0 x \\ &\quad + \int_0^x k_0(\epsilon_r - 1)\pi^{(2)}(\zeta) \sin k_0(x-\zeta)\, d\zeta \\ &\quad - \frac{1}{\omega}\frac{1}{Z_0} I_0 \operatorname{sgn}(x) \sin k_0 x \end{aligned} \tag{14}$$

where

$$Z_0 = \sqrt{\mu_0/\epsilon_0}$$

and

$$\operatorname{sgn}(x) = \begin{cases} 1, & \text{for } x > 0 \\ -1, & \text{for } x < 0. \end{cases}$$

A. Green's Functions for Both Regions

The Green's functions given below apply to regions 1 and 2 for case A and case B. The Green's functions for case B are given in Appendix I, those for free space (region (1)) are well known (see [4]).

1) Region 1—Half-Space $z \geqslant 0$: Subject to the assumption of a periodic field in this region, with periodic cell dimensions D_x and D_y defined in x and y directions

$$\begin{aligned}G^1(r, r') = -\frac{j}{D_x D_y}\sum_m\sum_n \frac{1}{K_{mn}} \exp\{-j[K_{mn}(z-z') \\ + k_0 u_m(x-x') + k_0 v_n(y-y')]\}\end{aligned} \tag{15}$$

where

$$K_{mn} = k_0\sqrt{1-u_m^2-v_n^2}, \qquad \text{for all integer } m, n \tag{16}$$

with the negative imaginary branch taken for negative argument and

$$u_m = u_0 + \frac{m\lambda}{D_x}; \quad v_n = v_0 + \frac{n\lambda}{D_y}.$$

2) Region 2—Case A: In the parallel plane region $-t \leqslant z \leqslant 0$ the fields have the same periodicity as $z > 0$. Since $E_y = 0$ at $z = -t$; the Green's function boundary condition is $\partial_z G(r, r') = 0$ at $z = -t$. In the expression below the source is set at $z' = 0$ (see Appendix)

$$\begin{aligned}G_A^{(2)} = -\frac{1}{D_x D_y}\sum_m\sum_n \frac{\cos K\epsilon_{mn}(z+t)}{K\epsilon_{mn} \sin (K\epsilon_{mn} t)} \\ \cdot \exp\{-jk_0[u_m(x-x') + v_n(y-y')]\}\end{aligned} \tag{17}$$

where

$$K\epsilon_{mn} = k_0\sqrt{\epsilon_r - u_m^2 - v_n^2}. \tag{18}$$

3) Region 2—Case B: When waveguide cavities are formed in the region $z < 0$ the solution in this region is required to satisfy the boundary conditions at the waveguide walls, as well as the base of the cavities ($z = -t$) (see Appendix).

The resulting Green's function is given below (for source location $z' = 0$).

$$\begin{aligned}G_B^{(2)} = -\frac{2}{d_x d_y}\sum_r\sum_q (2-\delta(q)) \frac{\cos k_z(z+t)}{k_z \sin k_z t} \\ \cdot \sin p\pi\left(\frac{x'}{d_x}+\frac{1}{2}\right) \sin p\pi\left(\frac{x}{d_x}+\frac{1}{2}\right) \\ \cdot \cos q\pi\left(\frac{y'}{d_y}+\frac{1}{2}\right) \cos q\pi\left(\frac{y}{d_y}+\frac{1}{2}\right)\end{aligned} \tag{19}$$

for $p = 1, 2 \cdots$; $q = 0, 1, 2 \cdots$ where

$$k_Z = k_0\sqrt{\epsilon_r - \left(\frac{p\lambda}{2d_x}\right)^2 - \left(\frac{q\lambda}{2d_y}\right)^2} \tag{20}$$

with the negative imaginary branch taken for negative argument.

Using the above Green's functions in the integral equations (13) completes the analytical formulation.

B. Reduction to the Final Matrix Equation

The system is reduced to a matrix equation by expanding the aperture field E_y in a series of sinusoids.

$$E_y = \sum_{i=1}^{I} A_i \sin i\pi(x/a + 1/2). \tag{21}$$

As indicated previously, the solution assumes thin slots, with no allowed field variation in the "y" direction. The constants C_1, C_2, and C_3 are also assumed independent of "y," and the "y" dependence present in the integral equations was removed by integrating the system of equations over the region $-b/2 \leqslant y \leqslant b/2$ (the slot width).

The series expansion results in algebraic equations to replace the integral equations (13). With the series truncated at $i = I$, there are $I + 3$ unknown constants. The final equations are as follows.

Case A

$$\begin{aligned} &C_1(1+\operatorname{sgn}(x))\cos k_0x + C_2 \sin k_0x \\ &+ C_3(1-\operatorname{sgn}(x))\cos k_0x + \sum_i^I A_i \frac{ba}{D_xD_y} \sum_m \sum_n \\ &\cdot [-\{jk_0(\epsilon_r-1)\gamma_m(x) + j\exp(-jk_0u_mx)\} \\ &\cdot \frac{\cot K\epsilon_{mn}(t)}{K\epsilon_{mn}} + \frac{1}{K_{mn}} \exp(-jk_0u_mx)] \\ &\cdot \eta_i(u_m, v_n)S_n = \operatorname{sgn}(x) I_0 \frac{\sin k_0x}{2} \end{aligned} \tag{22}$$

Case B

$$\begin{aligned} &C_1(1+\operatorname{sgn}(x))\cos k_0x + C_2 \sin k_0x \\ &+ C_3(1-\operatorname{sgn}(x))\cos k_0x + \sum_i^I A_i ba \left\{ \sum_m \sum_n S_n \right. \\ &\cdot \left[\frac{\eta_i(u_m, v_n)}{D_xD_yK_{mn}} \exp(-jk_0u_mx) \right] \\ &- j\frac{2}{d_xd_y} \sum_p \sum_q \left[\beta_i(p,q)(2-\delta(q)) \frac{\cot k_zt}{k_z} \right. \\ &\left. \left. \cdot \mathcal{S}_q(\sin p\pi \left(\frac{x}{d_x} + \frac{1}{2}\right) + k_0(\epsilon-1)\xi_p \right] \right\} \\ &= \operatorname{sgn}(x) Z_0 \frac{I_0}{2} \sin k_0x \end{aligned} \tag{23}$$

with the summation indices as defined for the Green's functions. The parameters, S, $\mathcal{S}$, ξ, η, β, and γ are defined in Appendix II.

The final step in converting these equations into matrix equations is to require them to be satisfied at $I + 3$ points within the region $a/2 \leqslant x \leqslant -a/2$. In this case, "$I$" was chosen odd, and the aperture points chosen equally spaced on each half of the aperture, starting at $x = \pm\epsilon$, for ϵ vanishingly small. The excitation I_0 was assumed unity.

C. Approximations and Series Convergence

Because of the large number of variables in this problem, it is necessary to choose to display data from only array lattice dimensions; so throughout the figures

$$D_x = D_y = d_x = d_y = 0.5\lambda$$

for Figs. 3, 4, 5, and 6. Figs. 7 and 8 show the results of using increased lattice dimensions

$$D_x = D_y = d_x = d_y = 0.55\lambda.$$

In all cases the slot thickness is $b = 0.05\ \lambda$.

The number of terms in the various series were varied to evaluate the convergence properties of each summation as well as of the matrix equation. It was found that the series in "m," "n," "p," and "q" (22) and (23) could be truncated at $m = n = p = q = 14$ with resulting conductance parameters differing from those computed for $m = n = p = q = 80$ by only a few percent for most of the cases tested. The value 20 was used throughout Figs. 5 and 6 except where indicated. Figs. 3, 4, 7, and 8 were computed with these series truncated at 14, to save computer time. Values of I up to 39 were used, but the general shape of the curves was unchanged once "I" was greater than about seven.

Several instances of "relative convergence" phenomena were observed for cases with a very thin layer of high dielectric material. This phenomenon is commonly encountered in the series solution of such problems in which the integral equation kernel is expanded as a truncated series (in this case using the indices p and q in one region, m and n in the other). As more terms are used to approximate the unknown, a point is reached beyond which further increases lead to severe divergence in the hitherto converging solution.

In the present study several examples of "relative convergence" [4] effects were observed for cases in which the parameter I substantially exceeded m, n, p or q, but for "I" less than or equal to these parameters the convergence was uniform except for the several cases with relative dielectric constant nine. In these cases there was good convergence for $I = 13$ or less. As will be indicated later, conservation of power was found to be a good measure of the stability of the solution (in the sense of its relative convergence). For this reason, two measures of power, the circuit power P and the radiated power P_t are defined in the next section. The validity of the solution was assured not only by noting convergence in the p, q, m, n, and I variables, but by comparing the two power measures as well in order to assure that the results were free of such relative convergence errors.

Near resonance, the radiation resistance R and the two power measures (P_z and P) described in the next section were stable, and not strongly dependent on any of the truncation parameters, while the reactance, conductance, and susceptance were more sensitive.

IV. Admittance, Impedance Radiated Power, and Element Patterns

The slot impedance is defined below, in terms of the total voltage v (the electric field integrated across the center of the slot and the applied current I_0

$$Z = \frac{V}{I_0} = \frac{b}{\lambda} \sum_{i=1,3,5} A_i. \tag{24}$$

Using this expression, one can write one form of the average radiated power for each slot as

$$P_z = \frac{1}{2}\,\mathrm{Re}\,(z) \quad \text{since } I_0 = 1. \tag{25}$$

A second definition of radiated power based upon integrated fields can be compared to (28). The average power per unit cell radiating in the normal direction away from the infinite array is

$$P = \int_{\text{cell}} \bar{S} \cdot \hat{z}\, ds \tag{26}$$

where $\bar{S}$ is the Poynting vector

$$\bar{S} = \frac{1}{2}\,\mathrm{Re}\,(E \times H^*) \tag{27}$$

so

$$P = \frac{1}{2}\,\mathrm{Re}\left\{\frac{j\omega}{\mu}\int_{\text{cell}} \partial_z \pi (\partial_{xx}^2 \pi^* + k_0^2 \pi^*)\right\}$$

$$= \frac{(ba)^2}{2Z_0 D_x D_y}\,\frac{(1-u_m^2)}{\sqrt{1-u_m^2-v_n^2}}\left|\sum_{i=1}^{I} A_i \eta_i(u_m, v_n)\right|^2.$$

This formula applies for any radiating mode $u_m^2 + v_n^2 < 1$. Z_0 is the free space impedance

$$(Z_0 = \sqrt{\mu_0/\epsilon_0}). \tag{28}$$

These two definitions of power were compared for all computed data. Except near pattern anomalies they were always within a few percent of each other as long as only a single mode radiates (no grating lobe). In those cases where "relative convergence" was a problem, a comparison of the results of (25) and (27) proved to be a sensitive measure of the overall stability of the solution.

Active element patterns are often used to illustrate the scanning properties of arrays when the admittance of the feeding transmission line is fixed, as in the case of waveguide radiators. They are less general than impedance or admittance plots in the present case, for one could choose to excite the slots by a number of different feed mechanisms or devices. For an infinite array the element pattern is cos θ multiplied by the array power transmission factor, which is the ratio of the power transmitted in a given direction to the input power (into a matched load). This definition implies that a characteristic load impedance is chosen for the feed circuit, and then the matched load input power is then the maximum power transmitted (or half the power in the circuit).

In order to compute the ratio of radiated power to that into a matched load, including the case when several grating lobes are present, an equivalent resistance is defined using the radiated power

$$R_{\text{eq}} = \frac{2P}{|I_0|^2} = 2P \tag{29}$$

using (25).

Based upon a series circuit equivalent, the ratio of power into the resistance R_{eq} to that into a matched load is

$$P_{\text{norm}} = \frac{4R_0 R_{\text{eq}}}{|R_0 + z|^2} \tag{30}$$

where R_0 is the characteristic transmission line impedance, chosen to match the antenna at some angle. Usually R_0 is selected for broadside match, by requiring $R_0 = R_{\text{eq}}$ at broadside. The impedance z in this formula is that evaluated from (24), and so includes the series impedance of any number of radiating grating lobes.

Since the resistance term R in the impedance z is not identical to R_{eq}, then P_{norm} is not quite unity at broadside. This error is also exhibited in the comparison of P_z and power (P), as mentioned earlier, and is corrected by use of higher order approximations to the truncated series solutions.

A. Admittance and Impedance at Broadside for Various Dielectric Substrates

In addition to evaluating the need to divide the array using cavities (case A versus case B) this paper addresses and compares the result of using various dielectric substrates beneath the slots. These effects are related primarily to the existence of cut-off or propagating higher order modes in the region beneath the ground plane, and again are best understood by considering cases A and B separately.

In both cases the region 1 Green's function is the same, and consists of a sum of propagating or nonpropagating modes of the periodic structure, sometimes called a grating lobe series. The condition that a mode radiate is that the mode have u_m, v_n coordinates in the region

$$u_m^2 + u_n^2 < 1 \tag{31}$$

or that the scan angle direction cosines lie within a unit circle. Fig. 2 shows the grating lobe lattice for an array with 0.5 λ spacing in both dimensions. The grating lobe locations are shown as dots, spaced two units apart in the u and v planes. With 0.5 λ spacing, only one grating lobe exists within the unit circle for any scan angle (see x on figure), and hence only the main beam of the array radiates.

For case A, the field expansion below the ground plane (region 2) also includes a similar set of spatial harmonic modes, but the use of a dielectric substrate below the ground plane results in a propagation constant $K\epsilon_{mn}$ (18) that allows propagating modes within a circle of radius $\sqrt{\epsilon_r}$, instead of unity (see Fig. 2 (case A)). This can be a dramatic increase in the number of propagating modes, and can make the behavior of the various array parameters extremely sensitive to frequency and array lattice dimensions. Of greater importance, however, is that each of these modes has different behavior with scan angle, and this will be shown to lead to severe array blindness or rapid change in input impedance as a function of scan angle. For example, if $\epsilon_r = 2.5$, with $D_x = 0.50\ \lambda$, a grating lobe occurs in the substrate for $\theta > 25°$, and for $\epsilon_r = 9$ there are grating lobes in the substrate even at broadside.

For case B the boundary between propagating and nonpropagating modes is independent of scan angle, for (20)

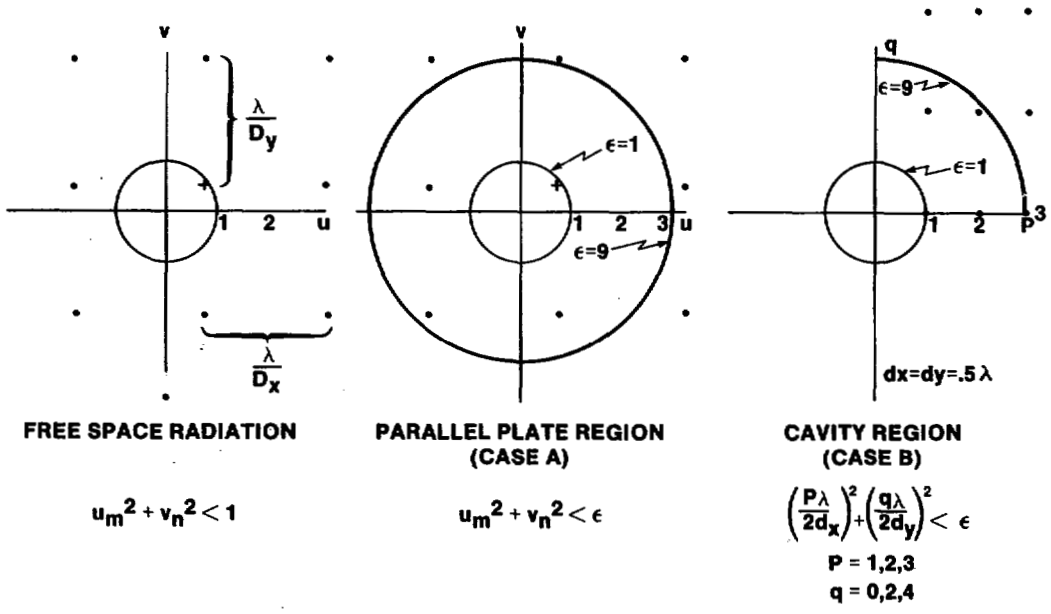

Fig. 2. Grating lobe and internal mode excitation.

shows that propagation in the waveguide cavity regions occurs from (p, q) such that

$$\epsilon_r > \left(\frac{p\lambda}{2d_x}\right)^2 + \left(\frac{q\lambda}{2d_y}\right)^2, \qquad \begin{matrix} p = 1, 2, 3 \cdots \\ q = 0, 2, 4. \end{matrix} \tag{32}$$

The set of p and q values that corresponds to radiating modes are shown within the circle of radius $\sqrt{\epsilon_r}$ in Fig. 2(b). Modes with q-odd are not excited.

If the cavity backed slot array (case B) has air dielectric or a very low dielectric constant substrate then it is usually possible to choose the cavity dimensions d_x and d_y so that a single mode propagates. This assures wider frequency performance and good scan characteristics. When high dielectric substrates are used, there may be many propagating modes because the radius of the circle (32) and Fig. 2 is still $\sqrt{\epsilon_r}$, but the mode propagation constants are independent of scan angle.

The substrate thickness "t" is usually chosen so that its electrical thickness is less than 0.25 wavelengths. For case A, $t/\lambda < 0.25/\sqrt{\epsilon_r}$, but for case B the value of t can be somewhat larger because of the elongated wavelength in the waveguide cavity region.

Admittance data are plotted throughout this paper because the slots appear naturally as shunt admittances in parallel with admittances of modes in the substrate region and because the slowly varying admittance data are more appropriate to plot than the series resonant impedance data.

At broadside, the variation of basic parameters is similar in cases A and B. The resonant slot dimension "a" varies with the dielectric constant ϵ, and the dimension t. Generally, decreasing the spacing "t" reduces the slot length at resonance, as shown in some of the examples in Figs. 3 and 4. However, when the dielectric constant is so large that several internal modes are present even at broadside, then the admittance curves are greatly modified, and no such simple dependence upon ϵ exists (Figs. 3(c), 4(b), and 4(c)). The location of the resonance is shown in these figures as the first zero crossing of the susceptance, as the dimension "a" is increased. At this point, the admittance changes from having an inductive (negative) susceptance to a capacitive (positive) susceptance.

The radiation resistance at resonance, however, is primarily a function of the slot dimension "a" is more important than the dielectric constant ϵ in determining the slot conductance. Since the resonance occurs for smaller "a" values when the dielectric constant is large, this leads to low conductance (high impedance) values for slots over high dielectric substrates.

B. Scanning Behavior—Element Patterns and Admittance

Figs. 5–8 detail the behavior of a number of slot arrays of the types designated case A (no cavities) or case B (with cavity separators). The figures show E- and H-plane (v and u-plane, respectively) normalized power transmission factors, which are readily converted to active element patterns upon multiplication by $\cos\theta$. These figures assume the characteristic impedances of the feed transmission lines chosen for broadside match. In each of these cases the normalized electrical thickness of the substrate is chosen equal to 0.2 λ at broadside for the lowest order mode in the substrate, which means that $t = 0.2\,\lambda_0/\sqrt{\epsilon_r}$ for case A, and

$$t = \frac{0.2\,\lambda}{\sqrt{\epsilon_r - \left(\frac{\lambda}{2d_x}\right)^2}} \tag{33}$$

for case B. Also, the slot length "a" for each case is chosen to resonate the array at broadside. This dimension, and the array broadside conductance, is given in the figure caption.

The figures indicate that all the case B results (with cavities) shown in Figs. 7 and 8 have u and v plane patterns that are nearly independent of the properties of the dielectric substrate, and that, for 0.5 λ spacing (Figs. 5 and 6) the u and v plane

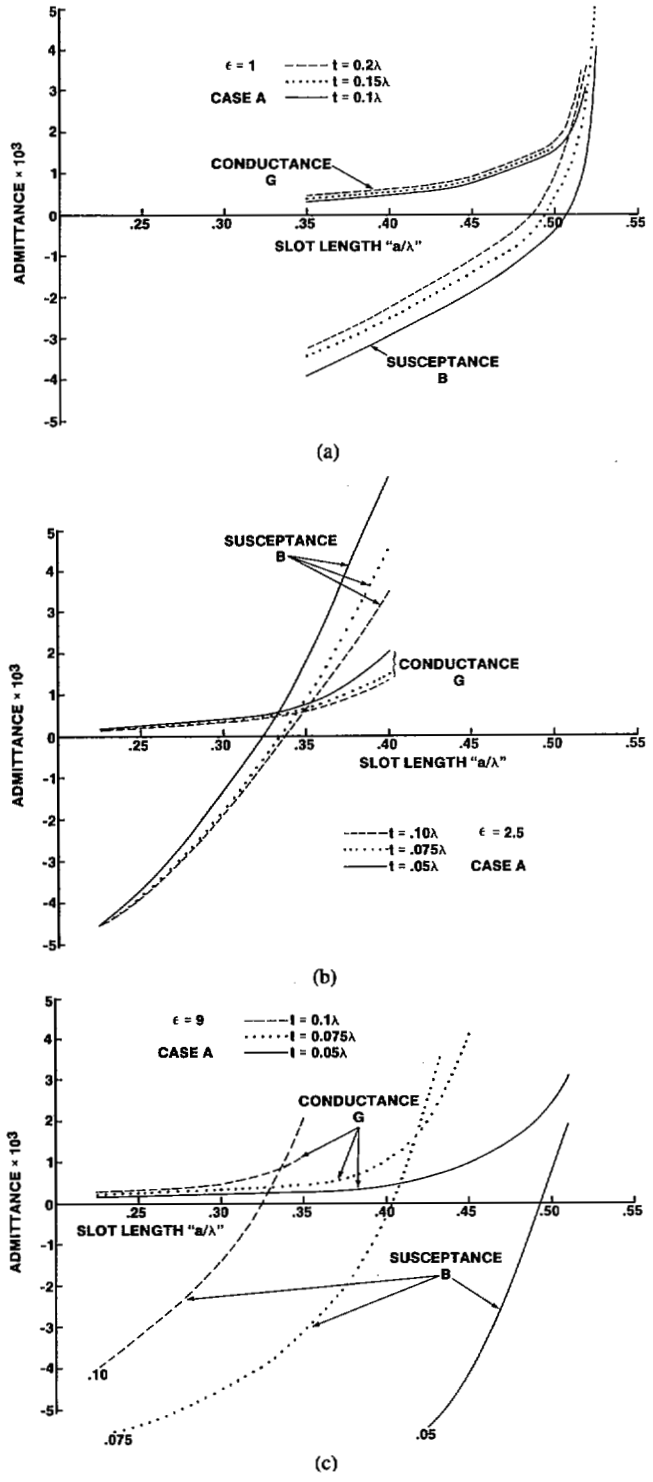

Fig. 3. Broadside admittance versus slot length for case A.

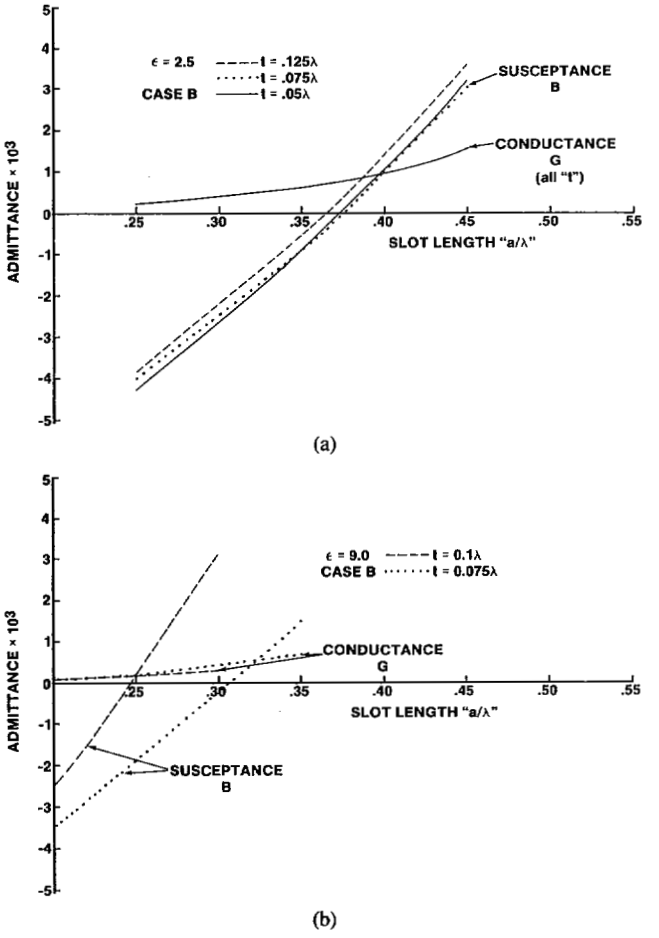

Fig. 4. Broadside admittance versus slot length for case B.

scan characteristics are nearly identical. In the case of 0.55 λ cell size the u and v patterns are different, as one would expect because of the emergence of the grating lobe at wider scan angles. For either spacing, the case B element patterns are wide and exhibit good scanning properties.

The case A results all have severely distorted element patterns and array blindness in either the u or v planes (or both) except for the air-filled case ($\epsilon_r = 1.0$). With $\epsilon_r = 2.5$, there is a severe blindness in the E plane (v plane) but none in the H-plane. This might suggest the possibility of building arrays with cavity separators in the E-plane only, but even this degree of simplification would not help for $\epsilon_r = 9$, where blindness occurs in both scan planes.

V. Conclusion

This paper has compared the radiation properties of slot arrays with and without separating cavities for various dielectric loadings and substrate thicknesses. The comparison was carried out using the same formulation, geometry and excitation for both cases, and this led to the use of idealized delta function current sources at each element.

The paper gives impedance parameters for a number of different array configurations, and shows a comparison of array scan parameters. The primary conclusion of this work is that except for arrays with air dielectric ($\epsilon_r = 1$) substrate, it is necessary to use separating cavities between slots.

Appendix I
Green's Functions in the Substrate (Region 2)

Case A

Assuming the same periodicity as above the substrate, we require

$$G_A^{(2)}(r, r') = \sum_m \sum_n A_{mn}(z) \exp\left[-jk_0(u_m x + v_n y)\right]. \quad (34)$$

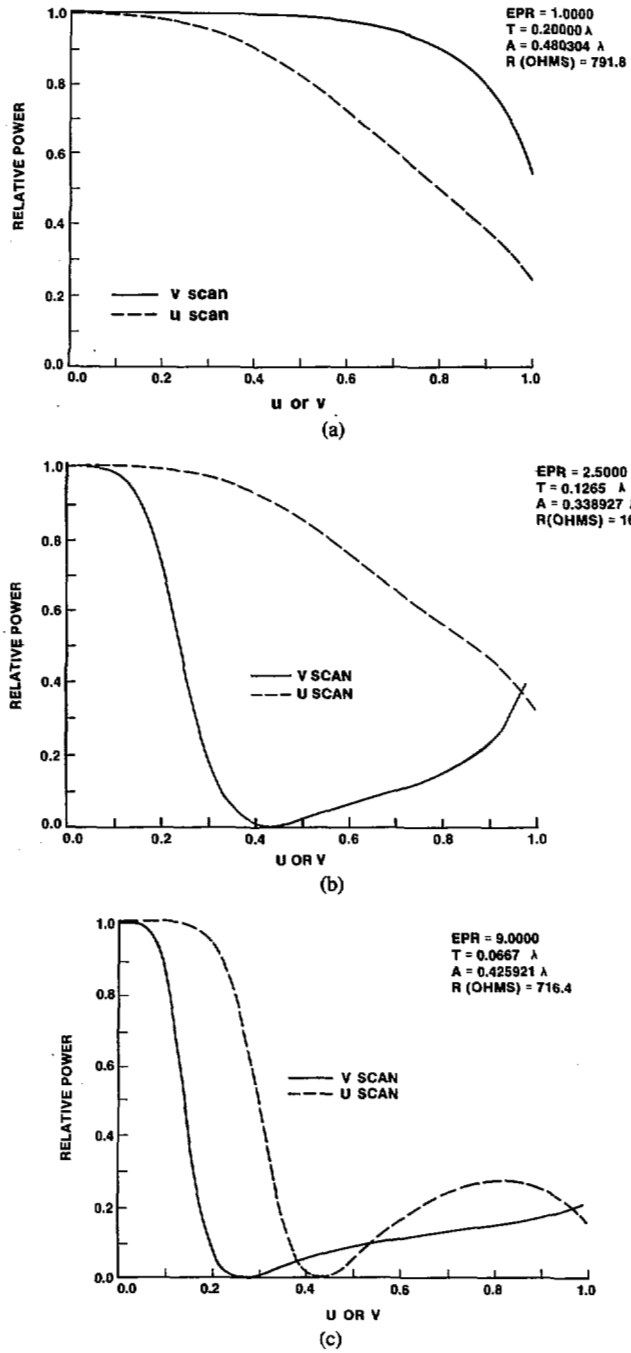

Fig. 5. Principal plane power transmission factor versus scan coordinates (u, v) for half-wavelength spacing (case A). Note: upper case dimensions are normalized to wavelength.

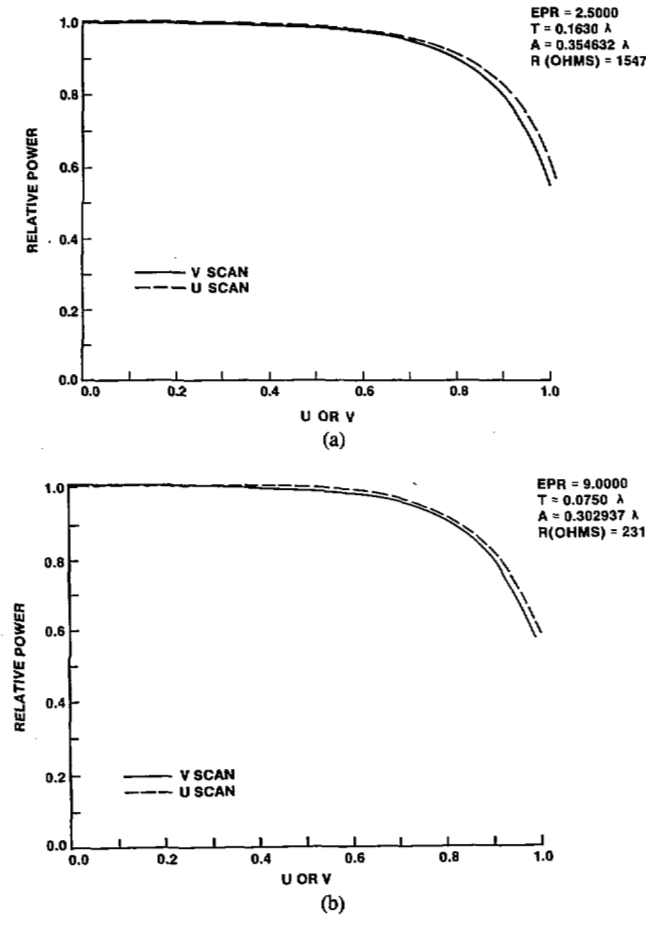

Fig. 6. Principal plane power transmission factor versus scan coordinates (u, v) for half-wavelength spacing (case B). Note: upper case dimensions are normalized to wavelength.

The Green's function solution must also satisfy $E_y \equiv 0$ at $z = -t$.

Starting with the inhomogeneous differential equation (6), substituting (1) above, multiplying by $e^{jk_0(u_m x + v_n y)}$ and integrating over a periodic cell, one obtains

$$(\partial_{zz}^2 + K\epsilon_{mn}^2)A_{mn}(z) = -\frac{\delta(z-z')}{D_x D_y}\exp\left[+jk_0(u_m x' + v_n y')\right] \tag{35}$$

where $K\epsilon_{mn}^2 = k_\epsilon^2 - k_0^2 u_m^2 - k_0^2 v_n^2$.

The z dependence is chosen to have vanishing normal derivative at $z = 0$ and $z = -t$; so is written below on either side of the source:

$$A_{mn}(z) = \begin{cases} D_{mn}\cos K\epsilon_{mn} z, & z > z' \\ E_{mn}\cos K\epsilon_{mn}(z+t), & z < z'. \end{cases} \tag{36}$$

Integrating the differential equation across a small region near the source evaluates the change in derivative

$$\partial_z A_{mn}(z)|_{z'+\sigma} - \partial_z A_{mn}(z)|_{z'-\sigma} = -\frac{1}{D_x D_y}\exp\left[jk_0(u_m x' + v_n y')\right]. \tag{37}$$

Using this condition and (3) for $A_{mn}(z)$, one obtains

$$-D_{mn}K\epsilon_{mn}\sin K_{\epsilon mn} z' + E_{mn}K\epsilon_{mn}\sin K\epsilon_{mn}(z'+t) = -\frac{\exp}{D_x D_y}\left[jk_0(u_m x' + v_n y')\right] \tag{38}$$

and from continuity of G at $z = z'$

$$D_{mn}\cos(K\epsilon_{mn} z') = E_{mn}\cos K\epsilon_{mn}(z'+t). \tag{39}$$

This allows evaluation of E_{mn} and D_{mn}. Since we will place

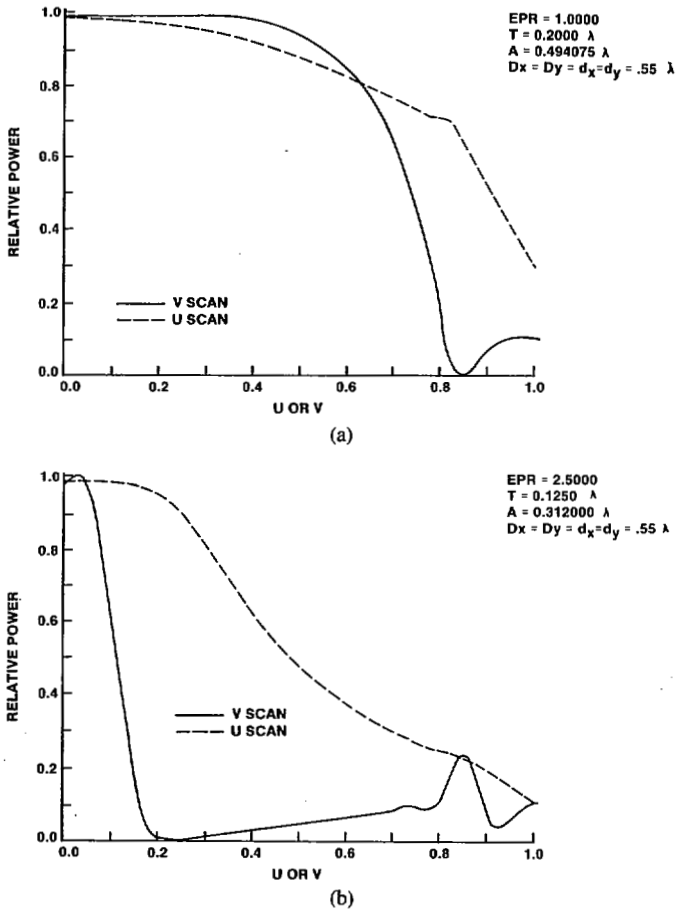

Fig. 7. Principal plane power transmission factor versus scan coordinates (u, v) for 0.55 wavelength spacing (case A).

the source at $z' = 0$, so only E_{mn} is needed

$$E_{mn} = \frac{-\exp\left[jk_0(u_m x' + v_n y')\right]}{K\epsilon_{mn}(\sin K\epsilon_{mn} t) D_x D_y}. \tag{40}$$

Equations (7) and (3), substituted into (1) of this Appendix yield the final expression for the case A Green's function, (17) in the main text.

Case B

The Green's function in the waveguide cavity loaded region is not periodic, but instead must satisfy the electromagnetic boundary conditions at the walls and bottom of each cavity, and also at $z = 0$.

Conditions on the E_y field require that the "z" derivative of the Green's function vanish at the cavity top and bottom ($z = 0$ and $-t$) and at the cavity side walls ($x = \pm d_x/2$) while the condition that $E = 0$ on all cavity walls adds the constraint that the normal ("y") derivative of the Green's function vanish at the cavity, walls ($y = \pm d_y/2$). The resulting Green's function has the form:

$$G_B^{(2)}(r, r') = \sum_{p=1}^{\infty}\sum_{q=0}^{\infty} g_{pq}(z) \cdot \sin p\pi\left(\frac{x}{d_x}+\frac{1}{2}\right)\cos q\pi\left(\frac{y}{d_y}+\frac{1}{2}\right). \tag{41}$$

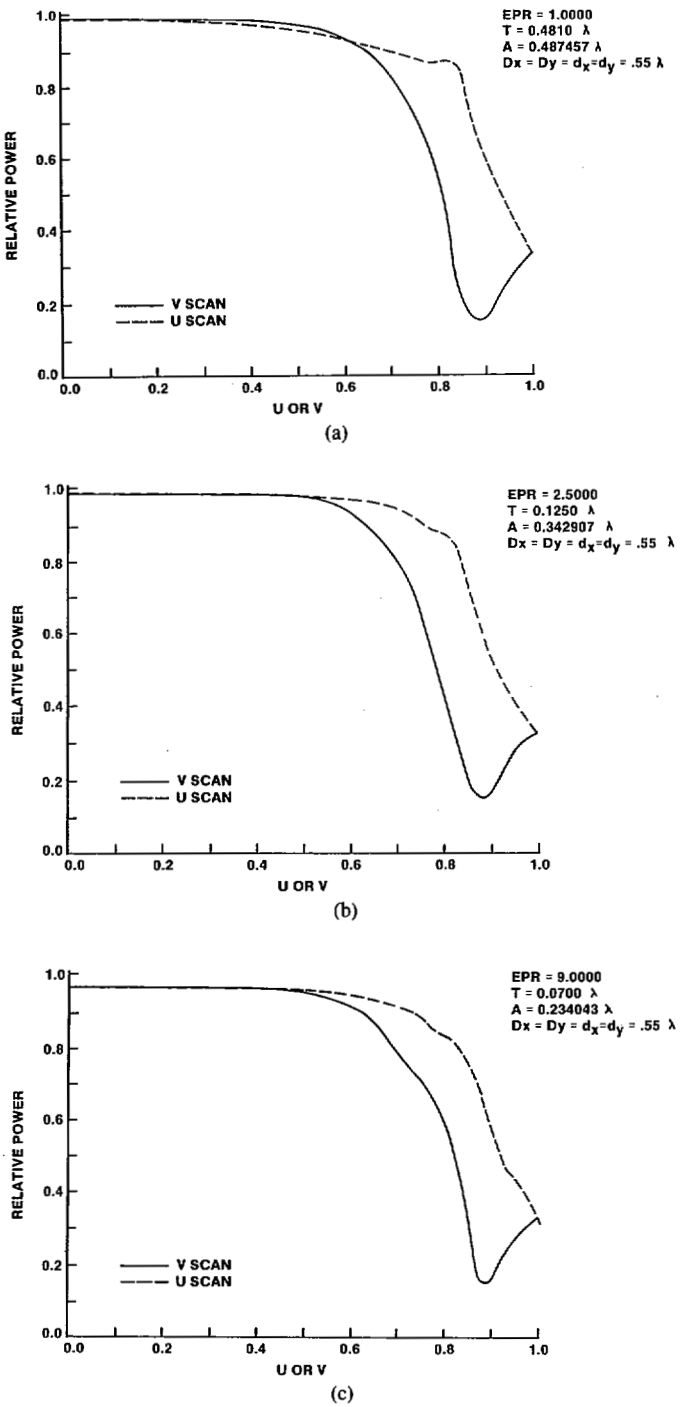

Fig. 8. Principal plane power transmission factor versus scan coordinates (u, v) for 0.55 wavelength spacing (case B).

As before, substituting the above into the inhomogeneous differential equation (1), using orthogonality of the sinusoidal functions and integrating over the waveguide cross section, one obtains

$$(\partial_{zz}^2 + k_z^2) g_{pq}(z) = -\frac{2}{d_x d_y}(2 - \delta(q)) \cdot \sin p\pi\left(\frac{x'}{d_x}+\frac{1}{2}\right)\cos q\pi\left(\frac{y'}{d_y}+\frac{1}{2}\right)\delta(z - z'). \tag{42}$$

Using

$$g_{pq}(z)=\begin{cases}F_{pq}\cos k_z z, & \text{for } z>z' \\ H_{pq}\cos k_z(z+t), & \text{for } z<z'\end{cases} \tag{43}$$

and the integral of the differential equation over the inhomogeneity, one obtains a relationship between the constants and H_{pq} and F_{pq}

$$\begin{aligned}\partial_z g_{pq}|_{z'+\sigma}-\partial_z g_{pq}|_{z'-\sigma} &= -k_z F_{pq}\sin k_z z' \\ &\quad + k_z H_{pq}\sin k_z(z'+t) \\ &= -\frac{2}{d_x d_y}(2-\delta(q))\sin p\pi\left(\frac{x'}{d_x}+\frac{1}{2}\right) \\ &\quad \cdot \cos q\pi\left(\frac{y'}{d_y}+\frac{1}{2}\right).\end{aligned} \tag{44}$$

Upon the use of the Green's function continuity condition

$$F_{pq}\cos k_z z = H_{pq}\cos k_z(z+t), \qquad \text{at } z=z'$$

and the relationship (44), one can solve for the unknown constants.

Since $z' = 0$, only H_{pq} is given below:

$$H_{pq}=\frac{-2(2-\delta(q))}{d_x d_y \sin k_z t}\sin p\pi\left(\frac{x'}{d_x}+\frac{1}{2}\right)\cos q\pi\left(\frac{y'}{d_y}+\frac{1}{2}\right).$$

The resulting Green's function is given in (19).

Appendix II

Definitions

The following expressions are defined for use in (25) and (26).

$$S_n=\frac{1}{b}\int_{-b/2}^{b/2}\exp\left[jk_0 v_n y'\right]dy'=\frac{\sin\left(k_0 v_n\frac{b}{2}\right)}{k_0 v_n b/2}$$

$$\begin{aligned}\eta_i(u_m, v_n) &= \frac{1}{ba}\int_{-a/2}^{a/2}\int_{-b/2}^{b/2}\exp\left[jk_0(u_m x' \right. \\ &\quad \left. + v_n y')\right]\sin i\pi\left(\frac{x'}{a}+\frac{1}{2}\right) \\ &= S_n\cdot\frac{2i\pi}{(i\pi)^2-(k_0 u_m a)^2} \\ &\quad \cdot\begin{cases}-j\sin k_0\mu_m\frac{a}{2}, & i \text{ even} \\ \cos k_0\mu_m\frac{a}{2}, & i \text{ odd}\end{cases}\end{aligned}$$

$$\begin{aligned}\beta_i(p, q) &= \frac{\delta q}{a}\int_{-a/2}^{a/2}dx'\sin p\pi\left(\frac{x'}{d_x}+\frac{1}{2}\right) \\ &\quad \cdot \sin i\pi\left(\frac{x'}{a}+\frac{1}{2}\right) \\ &= \frac{2\delta q}{\pi\left[\left(\frac{ap}{d_x}\right)^2-i^2\right]} \\ &\quad \cdot\begin{cases}(-1)^{p/2}i\sin\left(\frac{p\pi a}{2d_x}\right), & i, p \text{ even} \\ -(-1)^{(p-1)/2}i\cos\left(\frac{p\pi a}{2d_x}\right), & i, p \text{ odd} \\ 0, & \text{otherwise}\end{cases}\end{aligned}$$

where

$$\begin{aligned}\delta_q &= \frac{1}{b}\int_{-b/2}^{b/2}\cos q\pi\left[\frac{y'}{d_y}+\frac{1}{2}\right]dy' \\ &= \begin{cases}(-1)^{q/2}\sin\left(\frac{q\pi b}{2dy}\right), & q \text{ even} \\ 0, & q \text{ odd}\end{cases}\end{aligned}$$

$$\xi_p(x)=\int^x \sin p\pi\left(\frac{\zeta}{d_x}+\frac{1}{2}\right)\sin k_0(x-\zeta)\,d\zeta$$

$$= \begin{cases}(-1)^{p/2}\dfrac{\left[k_0\sin\frac{p\pi x}{d_x}-\left(\frac{p\pi}{d_x}\right)\sin k_0 x\right]}{k_0^2-\left(\frac{p\pi}{d_x}\right)^2}, & p \text{ even} \\ (-1)^{(p-1)/2}k_0\dfrac{\left[\cos\left(\frac{p\pi x}{d_x}\right)-\cos k_0 x\right]}{k_0^2-\left(\frac{p\pi}{d_x}\right)^2}, & p \text{ odd}\end{cases}$$

and

$$\begin{aligned}\gamma_m(x) &= \int_0^x \exp\left[-jk_0 u_m\zeta\right]\sin k_0(x-\zeta)\,d\zeta \\ &= \frac{1}{k_0}\left[\frac{1}{1-u_m^2}\right]\{\exp(-jk_0 u_m x) \\ &\quad + ju_m\sin k_0 x-\cos k_0 x\}.\end{aligned}$$

Acknowledgment

The author sincerely appreciates the conscientious efforts of Mr. E. Cohen of Arcon Corp., who wrote the computer programs for this analysis.

REFERENCES

[1] B. A. Munk, T. W. Kornbau, and R. D. Fulton, "Scan independent phased arrays," *Radio Sci.*, vol. 14, no. 6, pp. 979–990, Nov.-Dec. 1979.

[2] T. T. Wu, "Introduction to linear antennas," in *Antenna Theory*, pt. I, R. E. Collin and F. J. Zucker, Eds. New York: McGraw-Hill, 1969, ch. 8.

[3] J. Galejs, "Excitation of slots in a conducting screen above a lossy dielectric half space," *IEEE Trans. Antennas Propagat.*, vol. AP-10, pp. 436–443, July 1962.

[4] S. W. Lee, W. R. Jones, and J. J. Campbell, "Convergence of numerical solutions of iris-type discontinuity problems," *IEEE Trans. Microwave Theory Tech.*, vol. MTT-19, pp. 528–536, 1971.

[5] N. V. Shuley, "Relative convergence for moment-method solutions of integral equations of the first kind as applied to dichroic problems," *Electron. Lett.*, vol. 21, no. 3, pp. 95–97, Jan. 31, 1985.

[6] J. C. Herper, A. Hessel, and B. Tomasic, "Element pattern of an axial dipole in a cylindrical phased array, Part I: Theory," *IEEE Trans. Antennas Propagat.*, vol. AP-13, no. 3, pp. 259–272, Mar. 1985.

Robert J. Mailloux (S'57–M'66–SM'72–F'78) was born in Lynn, MA. He received the B.S. degree in electrical engineering from Northeastern University, Boston, MA, in 1961 and the S.M. and Ph.D. degrees from Harvard University, Cambridge, MA, in 1962 and 1965, respectively.

He was with the NASA Electronics Research Laboratories from 1970–1976. He is presently Chief of the Antenna Technology Branch, RADC, Electromagnetic Sciences Division, Hanscom AFB, Bedford, MA. His research interests are in the area of periodic structures and antenna arrays.

Dr. Mailloux is a member of Tau Beta Pi, Eta Kappa Nu, Sigma Xi, and Commission B of the International Union of Radio Science (URSI). He was a Distinguished Lecturer for the IEEE Antennas and Propagation Society (AP-S) during 1979–1981, Technical Activities Chairman for URSI Commission B and President of the Antennas and Propagation Society during 1983–1984. He is currently Chairman of the AP-S Long Range Planning Committee and a member of the Awards Committee.